

Adaptive Quantile Sparse Image (AQuaSI) Prior for Inverse Imaging Problems

Franziska Schirrmacher^{*,1}, Thomas Köhler^{*,1,2,3}, and Christian Riess¹

¹ Pattern Recognition Lab, FAU Erlangen-Nürnberg, Germany

² Erlangen Graduate School in Advanced Optical Technologies(SAOT), FAU
Erlangen-Nürnberg, Germany

³ e.solutions GmbH, Erlangen, Germany

* These authors contributed equally to this work.

Abstract. Inverse problems play a central role for many classical computer vision and image processing tasks. A key challenge in solving an inverse problem is to find an appropriate prior to convert an ill-posed problem into a well-posed task. Many of the existing priors, like total variation, are based on ad-hoc assumptions that have difficulties to represent the actual distribution of natural images.

In this work, we propose the Adaptive Quantile Sparse Image (AQuaSI) prior. It is based on a quantile filter, can be used as a joint filter on guidance data, and be readily plugged into a wide range of numerical optimization algorithms. We demonstrate the efficacy of the proposed prior in joint RGB/depth upsampling, on RGB/NIR image restoration, and in a comparison with related regularization by denoising approaches.

1 Introduction

In computer vision and image processing, many tasks are modeled as inverse problems ranging from low-level vision to image analysis and scene understanding. Inverse problems refer to the inference of latent information from noisy observations, whereas both quantities are linked by a generative model. For instance, in image denoising, we are interested in obtaining clean images from noisy ones under a certain noise model.

Despite widespread application domains, such formulations can be tackled by common tools from two complementary perspectives: *Model-based* approaches aim at inverting the generative model using iterative optimization techniques. This includes classical Bayesian statistics [1] or the most recent compressive sensing methodologies [2]. *Learning-based* approaches infer mappings in forward direction by learning from exemplars. Here, dictionary based methods [3] constitute the classical approach, while more recently deep neural network pushed the frontiers towards end-to-end learning, for example in super-resolution [4] or motion deblurring [5]. All of these strategies have in common that the underlying inverse problem is often highly *ill-posed*. This implies that its solution is not necessarily unique and continuously related to the given observations.

Turning ill-posed problems to well-posed ones requires task specific *priors* on the desired solution spaces. Such prior knowledge can be incorporated implicitly via learning from example data or explicitly by enforcing properties of a solution. The latter has the merit that it is exclusively driven by available input data without relying on external training data. It is achieved by a proper regularization of the problem, which can be steered by general assumptions like smoothness or sparsity of the desired solution. In computer vision, such priors are oftentimes justified by natural scene statistics, and are typically developed to make numerical optimizations tractable. We argue that such priors are too simplistic to reasonably model the appearance of natural images.

In this paper, we pursue the goal of designing a more appropriate model and propose the **Adaptive Quantile Sparse Image** (AQuaSI) prior – a novel prior for ill-posed inverse imaging problems. AQuaSI is based on the class of *weighted quantile filter* containing median filtering [6,7] as a special case, which is cast into a non-linear and sparsity-promoting regularizer. AQuaSI enables regularization via *joint filtering* by controlling the quantile filter kernel by guidance data in a spatially adaptive way. We further show that AQuaSI is universally usable and how it can be deployed in different model-based optimization approaches to solve typical inverse imaging problems¹. In different applications, including joint upsampling of RGB-D images and restoration of RGB/near infrared images, we demonstrate that our prior improves upon hand-crafted priors that are driven by ad-hoc assumptions.

2 Problem Statement and Related Work

In this paper, we investigate inverse problems in computer vision that deal with the recovery of a latent image denoted as a parameter vector $\mathbf{f} \in \mathbb{R}^n$ from measurements $\mathbf{g} \in \mathbb{R}^m$. We formulate such problems via energy minimization,

$$\hat{\mathbf{f}} = \operatorname{argmin}_{\mathbf{f}} \{ \mathcal{L}(\mathbf{f}, \mathbf{g}) + \lambda R(\mathbf{f}) \} \quad , \quad (1)$$

where $\mathcal{L}(\mathbf{f}, \mathbf{g})$ is a *data term* to measure the fidelity of \mathbf{f} with respect to \mathbf{g} under a given image formation model and $R(\mathbf{f})$ is a *regularization term* with weight $\lambda \geq 0$ derived from prior knowledge on the desired solution $\hat{\mathbf{f}}$. In common frameworks for denoising, deblurring, or super-resolution, we have $\mathcal{L}(\mathbf{f}) = \|\mathbf{g} - \mathbf{W}\mathbf{f}\|_2^2$, where $\mathbf{W} \in \mathbb{R}^{n \times m}$ is a task-dependent operator to implement an underlying linear image formation model. While the choice of the data term is application dependent, we focus on the design of a generic image prior to define $R(\mathbf{f})$.

Natural Scene Statistics and Sparsity Priors. The vast majority of classical image priors for Eq. 1 are derived from statistical models of natural scenes. Some common assumptions are to consider natural images as smooth, piecewise

¹ The source code to our methods will be made publicly available upon acceptance of the paper.

smooth, or piecewise constant signals under certain transforms. This includes the well known Total Variation (TV) prior [8] that has been widely adopted for image restoration. Many elaborated optimization frameworks exist to solve inverse problems with a TV prior, but the underlying statistical assumption of a piecewise constancy of image intensities is too simplistic to appropriately model the complex nature of natural scenes.

Further advances in the field of natural scene statistics led to Hyper-Laplacian priors [9,10,11], normalized scale-invariant priors [12], or non-linear extreme value priors like dark [13] or bright channels [14] specifically proposed for de-blurring. Such approaches exploit sparsity of natural images as a stronger prior for image restoration. Spectral priors [15,16] are likewise heading towards this direction but exploit low-rank properties of non-local similar patches. These are more suitable to model natural scene statistics but require specific optimization strategies like re-weighted minimization [10] or variable splitting [11], which limits their flexibility. We aim at designing an *out-of-the box* image prior that is widely applicable in conjunction with different optimization schemes.

Deep Learning Based Priors. The use of deep learning architectures like convolutional neural networks (CNNs) is a different track to design the prior in Eq. 1 and has become popular to solve low-level vision problems. In early works, classical approaches to sparse coding like [17] have been newly interpreted via CNNs and learned in an end-to-end fashion from exemplars [18]. Other approaches are to integrate denoising networks to regularize model-based optimization in variable splitting schemes [19,20]. However, these methods require learning from large-scale example datasets, which are not readily available in many real-world applications. In contrast, we propose an *unsupervised* prior.

Deep image priors [21] are one alternative as prior knowledge on natural images is extracted from network architectures rather than example data. In principle, this avoids the use of simplistic hand-crafted features for regularization but makes it difficult to deploy deep image priors in existing model-based image restoration frameworks.

Turning a Denoiser into a Regularizer. The most closely related strategies to ours formulate the prior in Eq. 1 via image denoising. Plug-and-Play priors [22,23] are one of the early approaches and replace shrinkage operators in variable splitting by invoking denoising algorithms. A more principled approach includes regularization by denoising [24] and considers clean images as a fixed point of image denoising. This allows the integration of many advanced denoising methods as prior knowledge to solve inverse imaging problems under different optimization frameworks. However, regularization by denoising is based on Tikhonov regularization, which can be expected to be less robust to, e. g., non-Gaussian noise than a L_1 -based regularizer.

3 Adaptive Quantile Sparse Image (AQuaSI) Prior

We now state the prior and its adaptive weighting, a linearization of the prior for optimization, then an example that relates AQuaSI to RED.

3.1 Definition of the Prior

As reviewed in Section 2, turning denoising algorithms into an image prior for regularization in Eq. 1 is an emerging topic in image restoration. Our approach follows a similar train of thought and is based on *weighted quantile filtering* as a particular denoiser. We denote a weighted p -quantile filter with $0 \leq p \leq 1$ for an image \mathbf{f} as $Q_{p,\mathbf{w}}(\mathbf{f})$, where $\mathbf{w} \in \mathbb{R}^N$ are spatially adaptive weights. Let $\mathbf{w}_i \in \mathbb{R}^n$ with $n = |\mathcal{N}(i)|$ be the weights within the kernel $\mathcal{N}(i)$ of this filter centered at the i -th pixel. Then, we define a permutation of these weights, $\tilde{\mathbf{w}}_i = m_i(\mathbf{w})$, such that the associated pixel intensities $m_i(f_{ij}) \in \mathcal{N}(i)$ are sorted in ascending order. The associated weighted p -quantile is the element $[Q_{p,\mathbf{w}}(\mathbf{f})]_i = f_z$ with

$$w_z = m_i^{-1}(\tilde{w}_{ik^*}) \quad \text{where} \quad k^* = \min k \quad \text{s.t.} \quad \sum_{j=1}^k \tilde{w}_{ij} \geq p \sum_{j=1}^n \tilde{w}_{ij} . \quad (2)$$

The general model in Eq. 2 is defined by the percentage parameter p that can be seen as a hyperparameter to adjust the filter for its desired application. One special instance of this model is the weighted median filter [6,7], where we have $p = 0.5$, which is particularly suitable for denoising under zero-mean noise.

Conceptionally, our proposed AQuaSI prior follows the idea that a natural image should be a fixed point under the weighted quantile filter². That is, given a clean image \mathbf{f} , we have for the *quantile residual* $\mathbf{f} - Q_{p,\mathbf{w}}(\mathbf{f}) = \mathbf{0}$. To deploy this approach for regularization of inverse problems, we relax this property and define our prior according to the sparsity inducing term

$$R_{\text{AQuaSI}}(\mathbf{f}) = \|\mathbf{f} - Q_{p,\mathbf{w}}(\mathbf{f})\|_1 . \quad (3)$$

3.2 Joint Filtering

Similar to existing local [7,25] or global optimization based methods [26], the proposed prior facilitates *joint filtering* by steering the regularizer in Eq. 3 with either internal or external image features. This is achieved by controlling the weights \mathbf{w} to define the kernel of the underlying weighted quantile operator. At the same time, the non-uniform choice of weights make the proposed technique spatially adaptive. More specifically, we determine the weight for the pixel f_j with respect to the pixel f_i for regularization of \mathbf{f} according to

$$w_{ij} = G_\sigma(z_i, z_j) , \quad (4)$$

² This assumption and the impact of different image degradations are further analyzed in the supplementary material.

where z_i and z_j are the respective pixels in a *guidance image* \mathbf{z} and $G_\sigma(z_i, z_j)$ measures their closeness. In Eq. 4, we use an isotropic Gaussian kernel

$$G_\sigma(z_i, z_j) = \exp\left(-\frac{(z_i - z_j)^2}{2\sigma^2}\right), \quad (5)$$

where σ is the standard deviation. We primarily distinguish between two modes for joint filtering: In a *static* guidance mode [7,25], we derive spatially adaptive weights from an external guidance image \mathbf{z} . In a *dynamic* guidance mode [26], spatially adaptive weights are internally derived in the domain of the regularized image without considering additional guidance data, i.e. $\mathbf{z} = \mathbf{f}$.

To show the impact of spatial adaptivity, we compare static and dynamic guidance to the so-called QuaSI prior [27], which is spatially constant (i.e., all weights are constant) on the publicly available *bowls* dataset [28]. The parameters of the proposed method are a $n = 5^2$ weighted median filter with $\sigma = 0.1$.

Figure 1 shows the results of this experiment. There is a difference between the results using the spatially constant prior and those using the *dynamic* guidance mode for the AQuaSI prior. Fine details, such as the border of the flower printing, are better preserved using the *dynamic* AQuaSI prior. The edges in Fig. 1f appear less blurred than the edges in Fig. 1c. Compared to the QuaSI prior, the *dynamic* AQuaSI prior preserves more details of the flower printing while smoothing homogeneous regions. Results are slightly smoother for *static* guidance mode when using intermediate results as guidance (Fig. 1e) than when using the noisy input image as guidance (Fig. 1d). Also the border of the flower printings are better preserved.

3.3 Pseudo-Linear Filtering

Our proposed prior in Eq. 3 is both non-convex and highly non-linear due to its underlying definition via weighted quantile filtering. This complicates numerical optimization when using this model for image restoration tasks. To mitigate this problem, a proper linearization can be used to deploy our prior for the solution of inverse imaging problems. In this paper, we propose to formulate $Q_{p,w}(\mathbf{f})$ in the pseudo-linear form [24]:

$$Q_{p,w}(\mathbf{f}) = \mathbf{Q}_\mathbf{f} \mathbf{f}, \quad (6)$$

where $\mathbf{Q}_\mathbf{f}$ denotes the weighted quantile filter in matrix notation constructed from the image \mathbf{f} . This decomposes our non-linear filter in the construction of its pseudo-linear form $\mathbf{Q}_\mathbf{f}$ adapted to the image \mathbf{f} and the actual filtering. While this formulation applies to many popular non-linear models like non-local means or bilateral filtering, the proposed weighted quantile filtering allows for the efficient linearization:

$$Q_{ij} = \begin{cases} 1 & \text{if } j = z \text{ in the sense of Eq. 2} \\ 0 & \text{otherwise} \end{cases}, \quad (7)$$

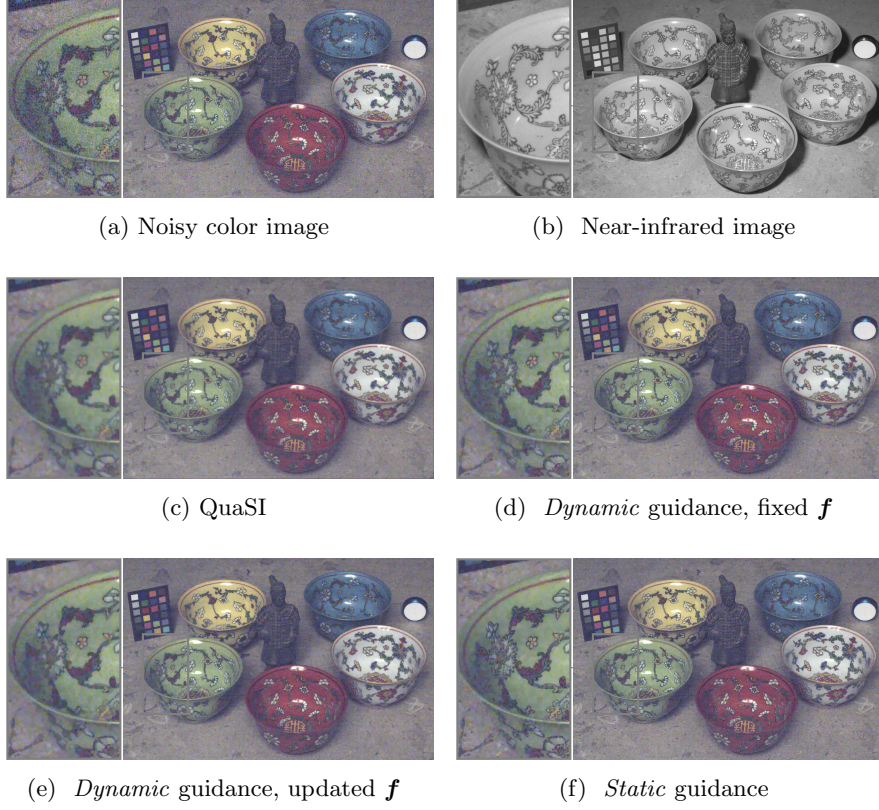


Fig. 1: Denoising the color image *bowls* [28] with the proposed algorithm using the ADMM optimization scheme in combination with the spatially non-adaptive QuaSI prior versus the two modes of the spatially adaptive AQuaSI prior.

where z denotes the position of the p -weighted quantile in the neighborhood $\mathcal{N}(i)$ centered at the i -th pixel.

The pseudo-linear form in Eq. 6 holds true for a fixed image \mathbf{f} . Let us now consider a perturbation of the image \mathbf{f} by a very small ϵ according to $\mathbf{f}' = \mathbf{f} + \epsilon$. Thus, we have the Taylor series expansion:

$$Q(\mathbf{f}') = Q(\mathbf{f} + \epsilon) = Q(\mathbf{f}) + \nabla_{\mathbf{f}}Q(\mathbf{f})\epsilon + \mathcal{O}(\epsilon^2) , \quad (8)$$

where $\nabla_{\mathbf{f}}Q(\mathbf{f})$ is the Jacobian of $Q(\mathbf{f})$ w. r. t. \mathbf{f} . Using the directional derivative property according to Romano *et al.* [24], we have $Q(\mathbf{f}) = \nabla_{\mathbf{f}}Q(\mathbf{f})\mathbf{f} = \mathbf{Q}_{\mathbf{f}}\mathbf{f}$. Then, we can approximate the above perturbation:

$$\begin{aligned} Q(\mathbf{f} + \epsilon) &\approx \nabla_{\mathbf{f}}Q(\mathbf{f})\mathbf{f} + \nabla_{\mathbf{f}}Q(\mathbf{f})\epsilon \\ &\approx \nabla_{\mathbf{f}}Q(\mathbf{f})(\mathbf{f} + \epsilon) \\ &= \mathbf{Q}_{\mathbf{f}}(\mathbf{f} + \epsilon) . \end{aligned} \quad (9)$$

Table 1: Comparison of the the proposed AQuaSI prior for non-blind deblurring with gradient descent optimization to regularization by denoising (RED) [24]. We evaluated deblurring under Gaussian and uniform blur kernels.

	RED [24] (Gaussian blur)	AQuaSI (Gaussian blur)	RED [24] (uniform blur)	AQuaSI (uniform blur)
PSNR	33.03	33.04	31.94	31.97
SSIM	0.98	0.98	0.98	0.98

This is quite useful as this derivation implies that we can use the linearization \mathbf{Q}_f to approximate the perturbation of the non-linear filter around \mathbf{f} for small ϵ . We extensively use this property in Section 4 to make numerical optimization with the AQuaSI prior tractable.

3.4 Comparison to Regularization by Denoising (RED)

AQuaSI is similar in spirit to regularization by denoising (RED) [24]. We investigate their relation on the evaluation image in the author’s software package. We use RED with the weighted median filter as denoising engine for the goal of deblurring. Blurring is applied to the ground truth color image, first with a 25×25 Gaussian PSF with $\sigma = 1.6$, and second with a 9×9 uniform point-spread function (PSF). Gaussian noise with a standard deviation of $\sqrt{2}$ is added to both images. To perform the comparison, we used the code of the authors and only replaced the RED prior by the AQuaSI prior. The parameters of the weighted median filter are set to $n = 9^2$ and $\sigma = 0.1$. Optimization (see Sec. 4.1) is performed with steepest descent with a fixed number of 20 iterations. PSNR and SSIM are computed relative to the ground truth color image. Table 1 shows the quantitative results. Both priors perform similarly, with a slight advantage of AQuaSI in the PSNR.

Figure 2 shows qualitative results. The blurred image is shown on the left, with Gaussian blur in the first row, and uniform blur in the second row. The results for RED and AQuaSI are shown in the middle and right columns, respectively. Qualitatively, the results of both regularization terms are comparable. Streak artifacts appear in the results with the uniform blur degradation model. The best deblurring and denoising performance is achieved with the Gaussian blur degradation model. Overall, it is important to note that Gaussian noise, as applied in the RED protocol, can very well be addressed by RED’s Tikhonov-based regularizer. However, it can be hypothesized that non-Gaussian noise opens an performance gap between the L_1 -based AQuaSI and the Tikhonov-based RED. Another major difference between the priors is in the computation time, since optimization of AQuaSI can omit updates of the pseudo-linear form \mathbf{Q}_f in some iterations (see Sec. 4.1). Here, we updated \mathbf{Q}_f in only every second iteration, which saves a factor of 2 on the runtime. Thus, computation of AQuaSI finishes in about 90 seconds while RED requires about 190 seconds.

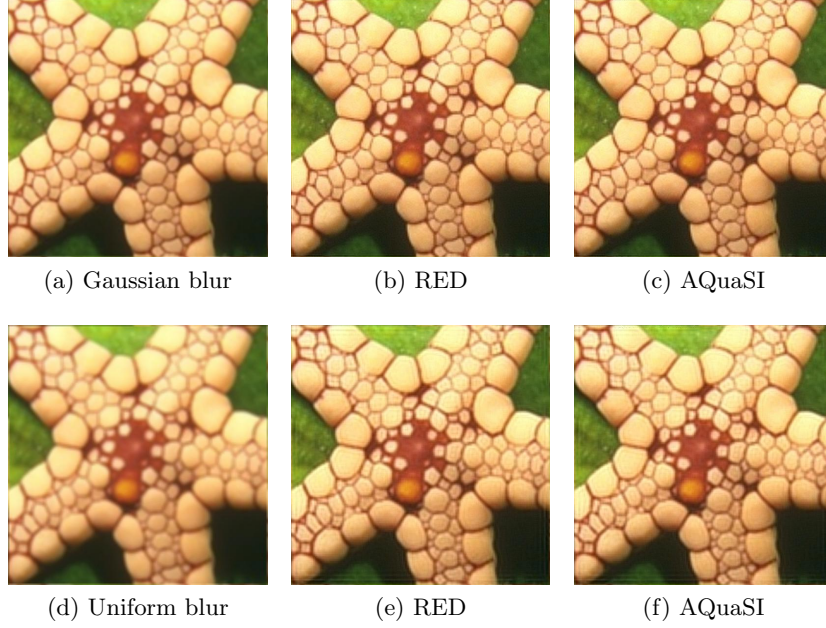


Fig. 2: Deblurring example. Top: Gaussian blur. Bottom: uniform blur. Left: input image. Middle: RED result. Right: AQuaSI result.

4 Numerical Optimization with AQuaSI Prior

In Section 3 we introduced our AQuaSI prior model and discussed several of its useful properties. Next, we show how this general model can be deployed within several numerical optimization schemes widely used to solve inverse imaging problems. We limit ourselves to iterative optimization algorithms that aim energy minimization under the general framework in Eq. 1.

4.1 Gradient Descent

Gradient descent based optimization methods are among the most frequently used approaches to solve inverse imaging problems. Let us study steepest descent as a conceptional simple yet flexible iteration scheme in this class. Given an estimate \mathbf{f}^t for the solution of the inverse problem in Eq. 1 with the problem specific data fidelity term $\mathcal{L}(\mathbf{f}, \mathbf{g})$, we refine \mathbf{f}^t from iteration t to $t+1$ according to the update equation

$$\mathbf{f}^{t+1} = \mathbf{f}^t - \mu \left(\nabla_{\mathbf{f}} \mathcal{L}(\mathbf{f}, \mathbf{g})|_{\mathbf{f}=\mathbf{f}^t} + \lambda \nabla_{\mathbf{f}} \| \mathbf{f} - Q_{p,w}(\mathbf{f}) \|_1|_{\mathbf{f}=\mathbf{f}^t} \right), \quad (10)$$

where $\nabla_{\mathbf{f}}$ denotes the gradient calculated at $\mathbf{f} = \mathbf{f}^t$ and μ is the step size parameter. In Eq. 10, we construct $Q_{p,w}(\mathbf{f})$ using the pseudo-linear form in Eq. 6

around the current estimate \mathbf{f}^t such that $Q_{p,w}(\mathbf{f}^t) = \mathbf{Q}^t \mathbf{f}^t$, where $\mathbf{Q}^t \equiv \mathbf{Q}_{\mathbf{f}^t}$. Based on this linearization, we calculate the gradient of the AQuaSI prior:

$$\nabla_{\mathbf{f}} \|\mathbf{f} - Q_{p,w}(\mathbf{f})\|_1 \big|_{\mathbf{f}=\mathbf{f}^t} = (\mathbf{I} - \mathbf{Q}^t)^\top \text{sign}(\mathbf{f} - \mathbf{Q}^t \mathbf{f}) . \quad (11)$$

To handle the non-differentiability of the L_1 norm at zero, we use an ϵ -smoothed version of the gradient where $\text{sign}(z) \approx z(\sqrt{z^2 + \epsilon})^{-1}$ for a small ϵ . The above iteration scheme can be employed with fixed step size parameter μ or line searches to determine μ dynamically per iteration. Moreover, we can revise the selection of the search direction from the steepest descent approach to related techniques like conjugate gradient (CG) iterations. To decrease the computation time, an update of \mathbf{Q}^t in every other iteration is sufficient. In this case, the pseudo-linear form is an approximation of the actual filtering.

4.2 Variable Splitting

We can also employ variable splitting techniques to approach the minimization of Eq. 1 with our AQuaSI prior. As one of the most popular techniques in this class of optimization schemes, we study the alternating direction method of multipliers (ADMM) [29], where Eq. 1 is rewritten as the constrained optimization problem:

$$(\hat{\mathbf{f}}, \hat{\mathbf{u}}) = \underset{\mathbf{f}, \mathbf{u}}{\text{argmin}} \{ \mathcal{L}(\mathbf{f}, \mathbf{g}) + \lambda \|\mathbf{u}\|_1 \} \quad \text{s.t. } \mathbf{u} = \mathbf{f} - Q_{p,w}(\mathbf{f}) \quad (12)$$

with the auxiliary variable \mathbf{u} . This equivalent to enforcing the non-linear constraint $\mathbf{u} = \mathbf{f} - Q_{p,w}(\mathbf{f})$ by minimizing the Augmented Lagrangian:

$$(\hat{\mathbf{f}}, \hat{\mathbf{u}}) = \underset{\mathbf{f}, \mathbf{u}}{\text{argmin}} \left\{ \mathcal{L}(\mathbf{f}, \mathbf{g}) + \lambda \|\mathbf{u}\|_1 + \frac{\alpha}{2} \|\mathbf{u} - \mathbf{f} + Q_{p,w}(\mathbf{f}) - \mathbf{b}_u\|_2^2 \right\} , \quad (13)$$

where α and \mathbf{b}_u denote the corresponding Lagrangian multiplier and a Bregman variable, respectively. In ADMM, the minimization of Eq. 13 is accomplished in an alternating manner according to

$$\mathbf{f}^{t+1} = \underset{\mathbf{f}}{\text{argmin}} \left\{ \mathcal{L}(\mathbf{f}, \mathbf{g}) + \frac{\alpha}{2} \|\mathbf{u}^t - \mathbf{f} + Q_{p,w}(\mathbf{f}) - \mathbf{b}_u^t\|_2^2 \right\} , \quad (14)$$

$$\mathbf{u}^{t+1} = \underset{\mathbf{u}}{\text{argmin}} \left\{ \lambda \|\mathbf{u}\|_1 + \frac{\alpha}{2} \|\mathbf{u} - \mathbf{f}^{t+1} + Q_{p,w}(\mathbf{f}^{t+1}) - \mathbf{b}_u^t\|_2^2 \right\} , \quad (15)$$

$$= \text{shrink} \left(\mathbf{f}^{t+1} + Q_{p,w}(\mathbf{f}^{t+1}) + \mathbf{b}_u^t, \frac{\lambda}{\alpha} \right) \quad (16)$$

$$\mathbf{b}_u^{t+1} = \mathbf{b}_u^t + (\mathbf{f}^{t+1} - Q_{p,w}(\mathbf{f}^{t+1}) - \mathbf{u}^{t+1}) , \quad (17)$$

where $\text{shrink}(z, \gamma) = \text{sign}(z) \max(z - \gamma, 0)$ is the shrinkage operator associated with the L_1 norm $\|\mathbf{u}\|_1$. For Eq. 14 - Eq. 17, we approximate $Q_{p,w}(\mathbf{f})$ by the pseudo-linear form in Eq. 6 similar to gradient descent. This can be done either by two linearization around \mathbf{f}^t (for Eq. 14) and \mathbf{f}^{t+1} (for Eq. 15 and Eq. 17) or a single linearization at \mathbf{f}^t for all update equations. We found that using a single linearization $Q_{p,w}(\mathbf{f}^t) = \mathbf{Q}^t \mathbf{f}^t$ for each pass of ADMM is sufficient, while using individual linearizations for each update equation is computationally more demanding.

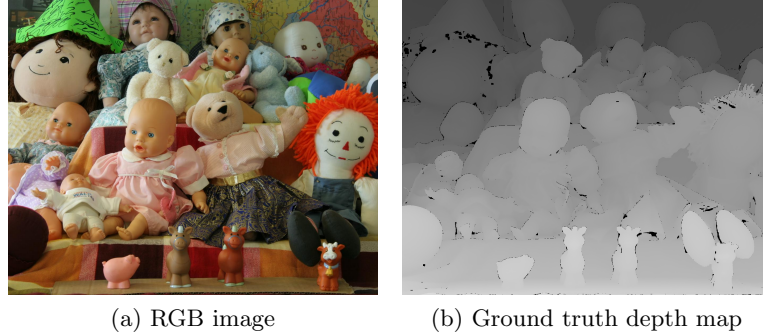


Fig. 3: RGB and depth map image pair from the Middlebury data set.

5 Applications

In order to emphasize the effectiveness of the AQuaSI prior, we evaluate the performance of the proposed method on two common inverse problems in computer vision, namely joint RGB/depth map upsampling and RGB/NIR image restoration. Additional implementation details on using our AQuaSI prior in these applications are reported in our supplementary material.

5.1 Joint Upsampling

The simulated Middlebury dataset provides pairs of color and depth map images [30]. We evaluate the performance of competing methods on the image pairs *Art*, *Books*, *Dolls*, *Laundry*, *Moebius* and *Reindeer*. Figure 3 shows the *Dolls* image pair. To generate the benchmark for joint upsampling, we applied Gaussian smoothing with $\sigma = 4$, nearest neighbor downsampling by a factor of 8, and added Gaussian noise with a standard deviation of 0.0005.

The performance is measured quantitatively using the Root Mean Square Error (RMSE) between the ground truth depth map and the algorithm result. Additionally, we report the Bad Matching Error (BME) [34]

$$E_{\text{BME}} = \frac{1}{N} \sum (|f_i - d_i| > \delta) , \quad (18)$$

where \mathbf{d} denotes the ground truth depth map, N are the number of pixels, and δ denotes a scalar that can be set accordingly.

To illustrate the effectiveness of the proposed AQuaSI prior, we use the prior as an additional regularization term for the SD filter [26]. The parameters of the AQuaSI prior were set to $p = 0.5$, $n = 9^2$, $\sigma = 0.1$, and $\lambda = 0.1$.

The results are compared to TGVL2 upsampling [32], the mutual structure filter (MS) [31], the deep joint filter (DJF), the residual-based deep joint filter (DJFR) [33], and the SD filter [26]. The parameter of the competing methods

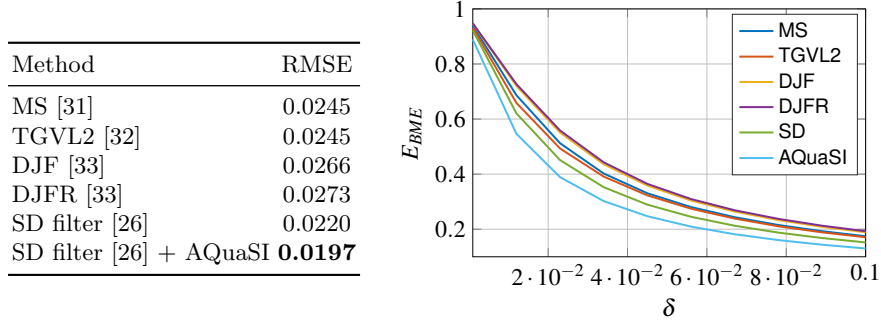


Fig. 4: Joint RGB/depth map upsampling using the state-of-the-art SD filter [26] augmented with our proposed AQuaSI prior. Left: root mean squared error (RMSE) achieved by the proposed method and several general-purpose (MS [31], DJF, and DJFR [33]) and customized RGB/depth map upsampling methods (TGVL2 [32]). Right: bad matching error (BME) at different thresholds δ .

were set according to suggestions of the authors. Figure 4 (left) lists the average RMSE over all image pairs. The combination of the SD filter with the AQuaSI prior yields the lowest RMSE. A reduction of the RMSE by 0.0023 is achieved through the AQuaSI prior compared to the SD filter only. Figure 4 (right) shows the mean BME relative to the ground truth depth map for different δ values. The AQuaSI prior further improves the results of the SD filter and outperforms all competing methods.

Figure 5 shows qualitative results of the competing methods. In the results of the mutual structure filter and the deep joint filter, noise is not suppressed very well. TGVL2 upsampling transfers too much structure from the color image to the depth map, which leads to artifacts. The combination of the SD filter with the AQuaSI prior achieves the best upsampling performance, which is consistent with the quantitative results. Compared to using the SD filter only, the AQuaSI prior greatly improves the results with respect to noise suppression and structure preservation.

5.2 RGB/NIR Cross Field Image Restoration

Another popular application for the proposed algorithm is color (RGB) and near-infrared (NIR) image restoration. The scene is captured using a RGB and a NIR camera. The task is to denoise the noisy color image using the NIR image as guidance. Due to the lower contrast and reversed edges in the NIR image, this presents a challenge for cross-field image restoration algorithms [35]. The results of the proposed method are compared to scale map [35] and the guided filter [25].

To quantify the performance in noise reduction after image restoration, we use the publicly available ARRI data set. The data set provides eleven ground

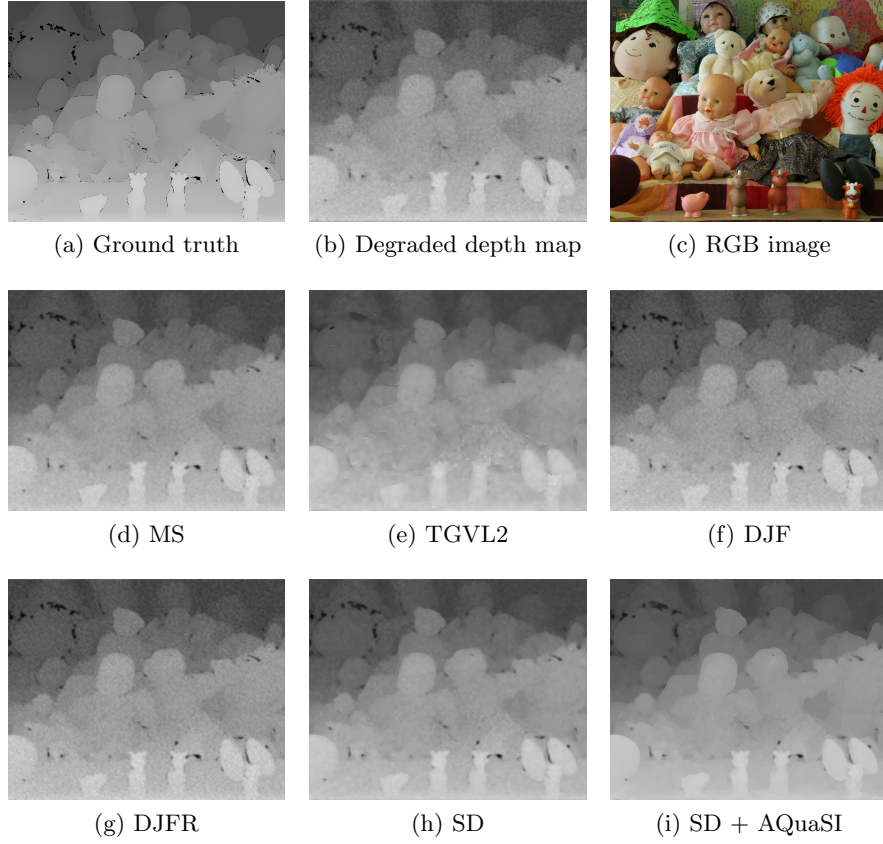


Fig. 5: Joint upsampling on the Middlebury image pair *Dolls*. (a) Ground truth depth map, (b) degraded depth map, (c) RGB image, (d) - (i) mutual structure (MS) filter, TGVL2 upsampling, deep joint filter (DJF), residual-based deep joint filter (DJFR), SD filter, and SD + AQuaSI.

truth RGB/NIR image pairs that are captured at the same instant of time and are well registered. The ARRI Alexa is a professional digital motion picture camera with a CMOS sensor in the APS-C format class. The NIR images are captured with the ARRI Alexa B&W. Both cameras were mounted on a mirror rig and the sensors were set on sensor sync for synchronization. Figure 6 shows an example image pair from the dataset. For evaluation, speckle noise with a standard deviation of $\sigma = 0.04$ is added to the noise-free RGB image.

We used the ADMM optimization from Section 4.2, and set the parameters to $\lambda = 23$, $\alpha = 2000$, $p = 0.5$, $n = 7^2$, $\sigma = 0.01$ and for an additional TV prior we chose $\mu = 0.4$ as regularization weight and $\beta = 30$ for the corresponding auxiliary variable.



Fig. 6: RGB/NIR image pair from the publicly available data set [36].

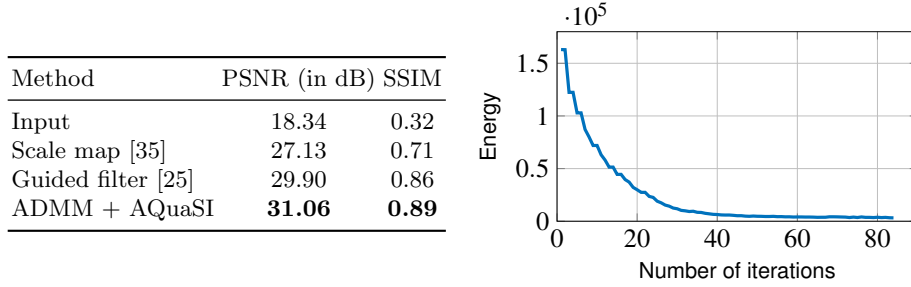


Fig. 7: RGB/NIR image restoration on the ARRI dataset. Left: comparison of ADMM optimization with the our AQuaSI prior to different state-of-the-art approaches to RGB/NIR restoration. Right: convergence of ADMM over the iterations (update of the AQuaSI pseudo-linear form after every second iteration).

Peak signal-to-noise ratio (PSNR) and structural similarity (SSIM) are computed to compare the performance of the proposed algorithm and state-of-the-art denoising methods. Figure 7 (left) lists the average PSNR and average SSIM value of all eleven image pairs for each method. The proposed AQuaSI prior shows the best results, with a PSNR of 31.06 compared to a PSNR of 29.90 for the guided filter [25] as the runner-up. Also the SSIM of 0.89 is best for AQuaSI, followed by the guided filter with a SSIM of 0.86.

The convergence of the proposed method using the ADMM optimization scheme with an update of \mathbf{Q}^t in every second iteration is shown experimentally. By our definition, the algorithm converges if a stationary point of the objective function in Eq. 1 is reached. The value of the objective, hereinafter referred to as energy, is computed after every update of the intermediate image \mathbf{f}^{t+1} . Figure 7 (right) shows the result of the experiment. The algorithm converges after 84 iterations and has a favorable convergence behavior.

Figure 8 shows qualitative results on this experiment. In the top row, ground truth and noisy image are shown, in the bottom row the results of the guided fil-

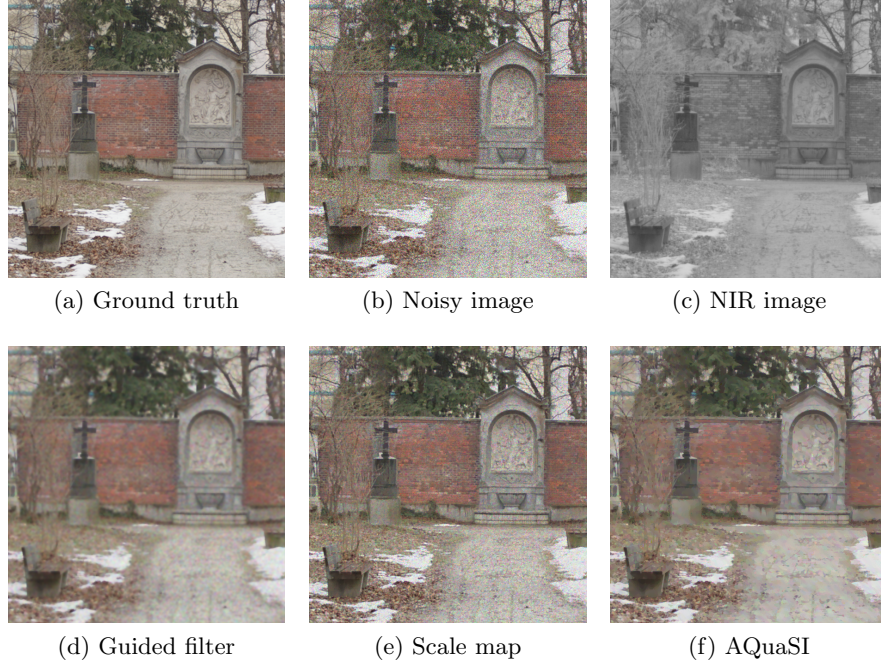


Fig. 8: RGB and NIR image restoration on the ARRI data set [36]. (a) Ground truth color image, (b) color image corrupted by speckle noise, (c) near-infrared (NIR) image, (d) - (f) guided filter, scale map and the proposed AQuaSI prior.

ter, scale map, and AQuaSI, respectively. The guided filter slightly oversmooths. Conversely, scale map produces a crisp output at the expense of colored noise, for example on the path. AQuaSI finds a good compromise between these two extremes, and produces overall a very satisfying result.

6 Conclusion

We propose AQuaSI, a novel prior for solving inverse problems. The key assumption of this prior is that good natural images are fixed points under a quantile filter with a spatially adaptive weighting scheme. The flexibility of AQuaSI can be attributed to the optional use of a guidance image, which can be either used in the direction of joint filtering based on a static guidance, or in the spirit of filtering with a dynamic guidance. We present AQuaSI within a full mathematical framework to linearize the proposed prior and to seamlessly integrate it into popular numerical optimization schemes such as gradient descent and ADMM.

In our experimental results, we demonstrate the strength of AQuaSI for the application of joint RGB/depth map upsampling, RGB/NIR image restoration, and in a direct comparison to the recently proposed regularization by denoising.

Our prior is universally applicable and compares favorably against the state-of-the-art in the investigated example applications.

References

1. Babacan, S.D., Molina, R., Katsaggelos, A.K.: Variational Bayesian Super Resolution. *IEEE Transactions on Image Processing* **20**(4) (April 2011) 984–999
2. Ochs, P., Dosovitskiy, A., Brox, T., Pock, T.: An Iterated L1 Algorithm for Non-smooth Non-convex Optimization in Computer Vision. In: *IEEE Conference on Computer Vision and Pattern Recognition (CVPR)*, Portland, OR, IEEE (June 2013) 1759–1766
3. Elad, M., Aharon, M.: Image denoising via sparse and redundant representation over learned dictionaries. *IEEE Transactions on Image Processing* **15**(12) (2006) 3736–3745
4. Kim, J., Lee, J.K., Lee, K.M.: Accurate Image Super-Resolution Using Very Deep Convolutional Networks. In: *IEEE Conference on Computer Vision and Pattern Recognition (CVPR)*, Las Vegas, NV, IEEE (June 2016) 1646–1654
5. Wieschollek, P., Hirsch, M., Scholkopf, B., Lensch, H.P.: Learning Blind Motion Deblurring. In: *International Conference on Computer Vision (ICCV)*. Volume 2017-Octob. (2017) 231–240
6. Ma, Z., He, K., Wei, Y., Sun, J., Wu, E.: Constant Time Weighted Median Filtering for Stereo Matching and Beyond. In: *International Conference on Computer Vision (ICCV)*, Sydney, Australia, IEEE (December 2013) 49–56
7. Zhang, Q., Xu, L., Jia, J.: 100+ Times Faster Weighted Median Filter (WMF). In: *IEEE Conference on Computer Vision and Pattern Recognition (CVPR)*, Columbus, OH, IEEE (2014) 2830–2837
8. Perrone, D., Favaro, P.: A Clearer Picture of Total Variation Blind Deconvolution. *IEEE Transactions on Pattern Analysis and Machine Intelligence* **38**(6) (June 2016) 1041–1055
9. Krishnan, D., Fergus, R.: Fast Image Deconvolution using Hyper-Laplacian Priors. In: *Advances in Neural Information Processing Systems (NIPS)*, Vancouver, Canada, Curran Associates, Inc. (December 2009) 1033–1041
10. Köhler, T., Huang, X., Schebesch, F., Aichert, A., Maier, A., Hornegger, J.: Robust Multiframe Super-Resolution Employing Iteratively Re-Weighted Minimization. *IEEE Transactions on Computational Imaging* **2**(1) (March 2016) 42 – 58
11. Pan, J., Hu, Z., Su, Z., Yang, M.H.: L 0 -Regularized Intensity and Gradient Prior for Deblurring Text Images and Beyond. *IEEE Transactions on Pattern Analysis and Machine Intelligence* **8828** (2016) 1–14
12. Krishnan, D., Tay, T., Fergus, R.: Blind deconvolution using a normalized sparsity measure. In: *Proceedings of the IEEE Computer Society Conference on Computer Vision and Pattern Recognition*. (2011) 233–240
13. Pan, J., Sun, D., Pfister, H., Yang, M.H.: Blind Image Deblurring Using Dark Channel Prior. In: *IEEE Conference on Computer Vision and Pattern Recognition (CVPR)*, Las Vegas, NV (June 2016) 1628–1638
14. Yan, Y., Ren, W., Guo, Y., Wang, R., Cao, X.: Image Deblurring via Extreme Channels Prior. In: *IEEE Conference on Computer Vision and Pattern Recognition (CVPR)*. (2017) 6978–6986
15. Wang, S., Zhang, L., Liang, Y.: Nonlocal spectral prior model for low-level vision. In: *Lecture Notes in Computer Science (including subseries Lecture Notes in*

- Artificial Intelligence and Lecture Notes in Bioinformatics). Volume 7726 LNCS. (2013) 231–244
16. Gu, S., Zhang, L., Zuo, W., Feng, X.: Weighted nuclear norm minimization with application to image denoising. In: IEEE Conference on Computer Vision and Pattern Recognition (CVPR). (2014) 2862–2869
 17. Yang, J., Wright, J., Huang, T.S., Ma, Y.: Image Super-Resolution via Sparse Representation. *IEEE Transactions on Image Processing* **19**(11) (November 2010) 2861–2873
 18. Wang, Z., Liu, D., Yang, J., Han, W., Huang, T.: Deep networks for image super-resolution with sparse prior. In: International Conference on Computer Vision (ICCV). Volume 2015 Inter. (2015) 370–378
 19. Zhang, K., Zuo, W., Gu, S., Zhang, L.: Learning deep cnn denoiser prior for image restoration. In: IEEE Conference on Computer Vision and Pattern Recognition (CVPR). (July 2017) 3929–3938
 20. Meinhardt, T., Moeller, M., Hazirbas, C., Cremers, D.: Learning Proximal Operators: Using Denoising Networks for Regularizing Inverse Imaging Problems. In: International Conference on Computer Vision (ICCV). Volume 2017-Octob. (2017) 1799–1808
 21. Ulyanov, D., Vedaldi, A., Lempitsky, V.S.: Deep image prior. *arXiv preprint arXiv:1711.10925* (2017)
 22. Venkatakrishnan, S.V., Bouman, C.A., Wohlberg, B.: Plug-and-Play priors for model based reconstruction. In: 2013 IEEE Global Conference on Signal and Information Processing, GlobalSIP 2013 - Proceedings. (2013) 945–948
 23. Chan, S.H., Wang, X., Elgendy, O.A.: Plug-and-Play ADMM for Image Restoration: Fixed Point Convergence and Applications. *IEEE Transactions on Computational Imaging* **3**(1) (2017) 84–98
 24. Romano, Y., Elad, M., Milanfar, P.: The Little Engine that Could: Regularization by Denoising (RED). *SIAM Journal on Imaging Sciences* **10**(4) (November 2017) 1804–1844
 25. He, K., Sun, J., Tang, X.: Guided Image Filtering. *IEEE Transactions on Pattern Analysis and Machine Intelligence* **35**(6) (June 2013) 1397–409
 26. Ham, B., Cho, M., Ponce, J.: Robust Image Filtering using Joint Static and Dynamic Guidance. In: IEEE Conference on Computer Vision and Pattern Recognition (CVPR), Boston, MA, IEEE (June 2015) 4823–4831
 27. Schirmmacher, F., Köhler, T., Lindenberger, T., Husvagt, L., Endres, J., Fujimoto, J.G., Hornegger, J., Dörfler, A., Hoelter, P., Maier, A.K.: Temporal and Volumetric Denoising via Quantile Sparse Image (QuaSI) Prior in Optical Coherence Tomography and Beyond. *ArXiv e-prints* (February 2018)
 28. Krishnan, D., Fergus, R.: Dark flash photography. In: ACM SIGGRAPH 2009 Papers. SIGGRAPH '09, ACM (2009) 96:1–96:11
 29. Goldstein, T., Osher, S.: The Split Bregman Method for L1-Regularized Problems. *SIAM Journal on Imaging Sciences* **2**(2) (January 2009) 323–343
 30. Scharstein, D., Pal, C.: Learning conditional random fields for stereo. In: 2007 IEEE Conference on Computer Vision and Pattern Recognition. (June 2007) 1–8
 31. Shen, X., Zhou, C., Xu, L., Jia, J.: Mutual-structure for joint filtering. In: 2015 IEEE International Conference on Computer Vision (ICCV). (2015) 3406–3414
 32. Ferstl, D., Reinbacher, C., Ranftl, R., Ruether, M., Bischof, H.: Image guided depth upsampling using anisotropic total generalized variation. In: 2013 IEEE International Conference on Computer Vision. (2013) 993–1000

33. Li, Y., Huang, J.B., Ahuja, N., Yang, M.H.: Deep joint image filtering. In: Computer Vision – ECCV 2016, Cham, Springer International Publishing (2016) 154–169
34. Scharstein, D., Szeliski, R., Zabih, R.: A taxonomy and evaluation of dense two-frame stereo correspondence algorithms. In: IEEE Workshop on Stereo and Multi-Baseline Vision. (2001) 131–140
35. Yan, Q., Shen, X., Xu, L., Zhuo, S., Zhang, X., Shen, L., Jia, J.: Cross-field joint image restoration via scale map. In: The IEEE International Conference on Computer Vision (ICCV). (December 2013)
36. Lüthen, J., Wörmann, J., Kleinsteuber, M., Steurer, J.: A rgb/nir data set for evaluating dehazing algorithms. *Electronic Imaging* **2017**(12) (2017) 79–87